

# High current ionic flows via ultra-fast lasers for fusion applications

Hartmut Ruhl and Georg Korn

*Marvel Fusion, Theresienhöhe 12, 80339 Munich, Germany*

---

## Abstract

In the present paper we introduce a new accelerator concept for ions. The accelerator is nano-structured and can consist of a range of materials. It is capable of generating large ionic currents at moderate ion energies. The nano-structures can be tailored towards the accelerator thus being capable of driving ion beams with very high efficiency. The accelerator is powered by laser arrays consisting of many repetitive and efficient lasers in the 100J range with ultra-short intense laser pulses. Combining nano-structures and the proposed ultra-short pulse lasers can lead to new levels of spatio-temporal control and energy efficiency for fusion applications.

*Keywords:* ionic implosion, nuclear fusion, embedded nano-structured acceleration, advanced laser arrays.

---

## Contents

<b>1 Introduction</b>	<b>1</b>
<b>2 The model</b>	<b>1</b>
<b>3 High efficiency ion acceleration</b>	<b>2</b>
<b>4 Conclusions</b>	<b>4</b>
<b>5 Acknowledgements</b>	<b>4</b>

### 1. Introduction

The indirect drive ICF approach has recently achieved an impressive milestone at NIF [1, 2, 3, 4, 5, 6, 7, 8, 9] demonstrating the principal viability of inertial confinement fusion for energy production. A detailed overview over ICF is given by [10].

The coupling efficiency of an external energy source to fusion fuels is a challenging problem. It is known that nano-structures can tailor and greatly enhance the coupling between lasers and matter via a range of interesting nonlinear optical effects [11, 12, 13, 14, 15, 16].

We propose an efficient ultra-high current accelerator composed of nano-structures driven by arrays of ultra-short intense laser pulses with potential applications in the context of ICF today and fusion with fuels with large activation energies in the future.

We show that the fuel velocities the accelerator can generate can be very high implying very high flow pressures. The accelerator is capable of spreading fluid densities and velocities. Hence, fuels with activation energies in the sub-MeV range may come within reach.

High power short pulse laser technology has made impressive progress over recent years [17, 18]. The total energy of the array of laser pulses is in the range of 10 – 100 kJ. Since the nano-structures in the accelerator can be tailored to the optical

laser radiation the coupling efficiency between the lasers and the embedded accelerator is extremely high.

The numerical model used in the paper is capable of separating the electronic time scales from the ones of the reactive ion flows in each segment of the electro - ionic model. The electronic parameters enter the ion flow equations as external parameters. Their correct values can be determined by appropriate self-consistent equations or parametrically depending on the computational load that can be afforded. This way the code can simulate the fast electron dominated accelerator and the reactive flow dynamics in the context of kinetic reactive fluid dynamics.

The intent of the present paper is to introduce a new acceleration concept for reactive fluids with a large range activation energies with the help of ultra-fast, highly efficient electromagnetic acceleration of ions. The acceleration process is based on nano-structures. The nano-structures are irradiated by intense short pulse lasers.

The paper is structured as follows. After stating the numerical model underlying our simulations in section 2 in some detail we explain the details of the accelerator concept in section 3. In section 4 we give a short summary and outlook.

### 2. The model

Since we are investigating ultra-fast electrons and fast high current reactive ionic flows in the context of fusion the fully relativistic numerical model underlying our investigations is kinetic and we base it on finite elements. While we do not make use of the reactive flow part of the numerical model in the present paper we quote some of its elements for future reference. The analytical abstraction underlying the kinetic reactive flows is outlined to some extent in [19]. The numerical model is an integrated adaptive multi-scale model making use of tree data structures to manage adaptive gridding and elements of machine learning to support feed forward error back integrators,

which allows the simultaneous investigation of the fast electronic as well as hydro time scales.

We obtain for  $k = 1, \dots, N$ , where  $N$  is the number of finite elements for the reactions

$$\frac{dn_k}{dt} \approx -n_k \sum_{l=1}^N n_l u_{kl} \sigma_R^{kl}(u_{kl}) \delta_{\vec{r}_k, \vec{r}_l} \quad (1)$$

and the equations of motion

$$\frac{d\vec{r}_k}{dt} \approx \vec{u}_k, \quad (2)$$

$$\frac{d\vec{p}_k}{dt} \approx \frac{q_k}{V} \int_V d^3r \phi(\vec{r}, \vec{r}_k) (\vec{E}_k + \vec{u}_k \times \vec{B}_k) - \sum_{l=1}^N \nu_{kl}(u_{kl}) (\vec{p}_k - \vec{p}_{kl}^s) \delta_{\vec{r}_k, \vec{r}_l}. \quad (3)$$

The equations and the symbols used are self-explanatory. The parameter  $\sigma_R^{kl}$  is the reactive cross section. The function  $\phi$  denotes the form factor of a finite element. Each finite element has the same density  $n_0$ . The remaining parameters to augment the force equations are

$$\nu_{kl}(u_{kl}) \approx \frac{n_l}{C_{kl} \gamma_{kl}^2 u_{kl}^3} \Lambda_{kl}, \quad (4)$$

$$\Lambda_{kl} \approx \ln\left(\frac{u_{kl}^2 + B}{B}\right) - \frac{u_{kl}^2}{u_{kl}^2 + B}, \quad (5)$$

$$C_{kl} = \frac{4\pi\epsilon_0^2 m_{kl}^2}{q_k^2 q_l^2}, \quad (6)$$

$$m_{kl} = \frac{m_k m_l}{m_k + m_l}. \quad (7)$$

The parameter  $B$  is an effective shielding parameter. The remaining kinematic relations are

$$\vec{u}_k = \frac{c\vec{p}_k}{\sqrt{m_k^2 c^2 + \vec{p}_k^2}}, \quad (8)$$

$$u_{kl} = \frac{c\sqrt{(p_k \cdot p_l)^2 - m_k^2 m_l^2 c^4}}{p_k^{0i} p_l^{0j}}, \quad (9)$$

$$\vec{p}_{kl}^s = \gamma_{kl} \vec{\beta}_{kl} p_k^0 - \frac{1}{\beta_{kl}^2} (\gamma_{kl} - 1) (\vec{p}_k \cdot \vec{\beta}_{kl}) \vec{\beta}_{kl}, \quad (10)$$

$$\vec{\beta}_{kl} = \frac{\vec{p}_k + \vec{p}_l}{p_k^0 + p_l^0}, \quad (11)$$

$$\gamma_{kl} = \frac{1}{\sqrt{1 - \beta_{kl}^2}}, \quad (12)$$

where care has to be taken if one of the colliding constituents is an electron. For the sake of brevity we do not state details.

Equations (1) - (7) are obtained by decomposing the reactive kinetic equations into reactive resistive motion and kinetic lateral broadening of the binary correlation operators. We do not quote the lateral broadening part of the model here. We note that lateral broadening is quite important for energy - momentum conservation. Neglecting it underestimates range, a

typical parameter in reactive flows. In addition, to include radiative processes we have to add radiation reactive terms on the mean field level of the model. On the binary correlation level the binary transition amplitudes have to be generalized to the radiative one. Equations (1) - (7) are augmented with Maxwell's equations.

### 3. High efficiency ion acceleration

A concern is the efficiency of the indirect drive ICF approach to fusion. We propose an embedded accelerator technology for fluids that makes use of embedded nano-structured accelerator configurations for the acceleration, convergence, and if required the divergence of ionic flows at very high efficiency and precision.

The configuration is powered by an array of efficient short-pulse lasers with moderate individual pulse energies in the range of 100J. They can generate ion kinetic pressures and convergence velocities that are orders of magnitude higher than what is state of the art at present.

The coupling between the laser pulses and appropriately tailored nano-rods can be extremely efficient. It is important to note in the context that the observed efficient laser - rod coupling is only possible because advanced laser pulse technology exists. The laser pulses this technology provides are capable of propagating into tailored configurations of nano-rods at the speed of light outrunning the impact of their interaction with the rods. Hence, the nano-structures cannot shield themselves from the absorption of the related extreme energy densities. By combining nano-structures and the proposed laser arrays a high degree of spatio-temporal control over the deployment of extreme optical energy densities on the fastest possible time scales in the accelerator at high efficiency levels can be expected.

For reasons of simplicity we stick to a cylindrical macro accelerator geometry in this paper, while the nano-rod simulations are fully 3D. The 2D accelerator layout is sketched in Fig. 1. Also a hypothetical 3D accelerator layout is sketched in the figure. The accelerator is comprised of multiple segments of nano-structured elements colored in blue in the figure. The nano-structured segments are irradiated by multiple laser pulses as depicted in the figure. Each laser pulse is capable of irradiating between  $10^8 - 10^9$  nano-structures. Each single irradiated nano-rod is capable of releasing up to  $10^{10}$  accelerated ions. The macro accelerator is capable of generating currents between  $10^{18} - 10^{19}$  ions in about 500 fs. The number of individual lasers in the array is about 1000. The required energies of the ions range between 0.1 - 2.0 MeV.

The expected ionic implosion velocities and flow pressures are orders of magnitude larger than those achievable with thermal ablation. There are conceptual similarities with the direct drive ICF approach [20]. Only the energy densities and spatio-temporal parameters achievable in the realm of fusion with advanced laser technology are orders of magnitude larger.

In Fig. 2 the ion energies obtained from a single nano-rod with varying radii interacting with short laser pulses up to 30 fs FWHM at  $\lambda = 400$  nm at the intensities of  $I_{<} \approx 1.0 \cdot 10^{21}$  Wcm<sup>-2</sup>

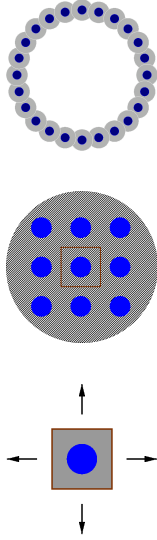


Figure 1: Sketch the hypothetical 2D accelerator and the irradiation pattern by the proposed multi-lasers (plot at the top), the irradiated elements of the accelerator (2nd from top), and the simulation box for the laser - rod interaction (bottom plot). The nano-rods are depicted in blue, the multi-lasers in shades of gray, and the simulation box boundaries in brown. To reduce computational load we take a single rod and periodic lateral boundaries in an effort to mimic the mutual correlations between the rods. Each laser pulse irradiates between  $10^8 - 10^9$  nano-rods depending of their setup. The accelerator contains up to  $10^{10}$  nano-structures. For the nano-geometry of the rods depicted and the morphology simulated the ion beam is launched in radial direction. However, the launch direction of individual fluids is a free parameter. The center of mass of the accelerator must remain at rest.

and  $I_{>} \approx 5.0 \cdot 10^{21} \text{ Wcm}^{-2}$  are shown. The simulated rod contains the same uniform number densities  $n_p = n_B = 10^{23} \text{ cm}^{-3}$  for protons and boron. The simulated rod is  $16 \mu\text{m}$  long, while the simulation box is  $32 \mu\text{m}$  long. The lateral boundary conditions are periodic, while front and back sides of the box are transparent. The numerical resolution is  $\Delta x = \Delta y = \Delta z = 5.0 \text{ nm}$ . The temporal resolution is about  $\Delta t \approx 7.2 \text{ as}$ .

A prominent feature in Fig. 2 is the convergence of the single particle energies of the protons and the boron ions to the same values for the two intensities  $I_{<}$  and  $I_{>}$  for rod radii  $R < 40 \text{ nm}$ . The process underlying the acceleration of the protons and the boron ions for the rod radii  $R < 40 \text{ nm}$  are Coulomb explosions. For large rod radii the conversion efficiency of the laser energy to the ions is small as expected since large rod radii exceed the skin depth by far. Since the energies of the protons and the boron ions are about the same for both intensities the energy conversion efficiency into ion energy increases more than 5-fold for the lower laser intensity since also the energy deposited into the electrons drops substantially at the lower intensity  $I_{<}$ . The implication is that nano-rods can be engineered to accommodate the desired nonlinear optical properties for the driver lasers and to transfer as much energy to the ions as possible while limiting electron energies. In Fig. 2 it is shown that there is an energy gap between the protons and the boron ions. The boron ions are about 3-fold as energetic as the protons. This observation can be understood taking the charged fluid expansion into account. The theoretically predicted factor is about 3.5 due

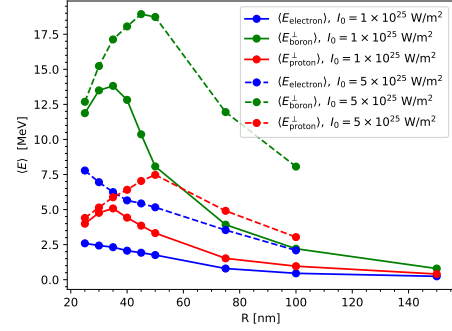


Figure 2: Illustration of the explosion of a single nano-rod exposed to an ultra-short high-field laser pulse with up to 30 fs FWHM at  $\lambda = 400 \text{ nm}$ . The figure shows the energy of the individual ions. Their energies can be tailored towards the peak of the fusion cross sections. The x-axis shows the radii of the simulated rods. The y-axis gives the energy per charged particle. The rods consist of a heavy substrate and a lighter reactive fluid. The substrate in the simulation is  $^{11}\text{B}$  and the light fluid consists of protons. By reducing the radii of the rods, their morphology, and the laser intensity less energetic ions can be generated. To emulate the interaction with multiple nano-rods periodic boundaries have been chosen as detailed in the text.

to the particular shape, size and composition of the rods. In important conclusion is that the energy gap between fluids from rod with multi ionic constituents can be engineered.

In Fig. 3 the energy balance in the simulation box as a function of the interaction time is monitored. The figure illustrates that there is a linear rise of the total ion energy for both the protons and the boron ions starting at about  $t = 25 \text{ fs}$  until at about  $t = 75 \text{ fs}$ . This corresponds to the time the impinging laser pulse needs to travel a length of  $16 \mu\text{m}$  at speed of light. At  $t = 25 \text{ fs}$  the laser pulse hits the nano-rod and at  $t = 75 \text{ fs}$  it leaves the rod. At  $t = 100 \text{ fs}$  the laser pulse exits the simulation box, which implies that the electromagnetic energy density in the simulation box must drop rapidly. The total energy in the simulation box is now in the ions and electrons with only little field energy left. The implication is that the system of charged particles is quasi-neutral at this point. The simulation is stopped at  $t = 200 \text{ fs}$ . It is apparent from the figure that the ions retain their kinetic energies while the electrons loose some of theirs since some of them exit the transparent front and back faces of the simulation box due to the specific numerical boundaries set up there. From Fig. 3 we conclude that  $> 60 \%$  of the deposited laser energy has been converted to the ions. We note that similar efficiency results should hold for somewhat longer laser pulses since the rods can be tailored towards the incident laser radiation.

Figure 4 shows the simulated proton and borons spectra for a rod with  $R = 25 \text{ nm}$  and for the intensity  $I_{<}$ . While the spectrum of the protons is sharply peaked at about  $4 \text{ MeV}$  the boron ion spectrum is broad. This leads to the separation of proton and boron fluids preventing thermalization between the species during rapid convergence. Making use of lower laser intensities and optimized rod morphologies the energy convergence efficiency and spectral signatures of both fluids can be considerably improved further.

Sketches of a few principal accelerator configurations in-

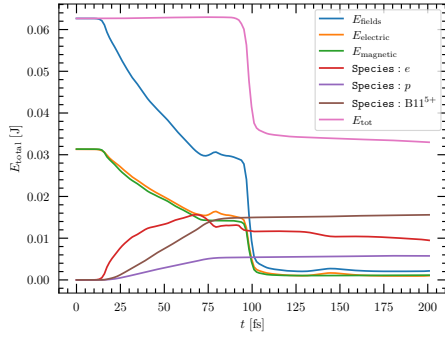


Figure 3: Illustration of the energy balance in the simulation box. Shown are the electromagnetic field energies, the electron energy, and the proton and boron energies as functions of time. As is seen both the proton and boron energies grow linearly with time and hence laser propagation depth. A second implication is that the nonlinear optical properties of the system seem to be under control. A third feature is the energy conversion efficiency into ions, which according to the figure is  $> 60\%$ . Almost the total absorbed laser energy is transformed into ionic motion. A total of about  $10^{10}$  ions are accelerated. The simulation parameters are detailed in the text.

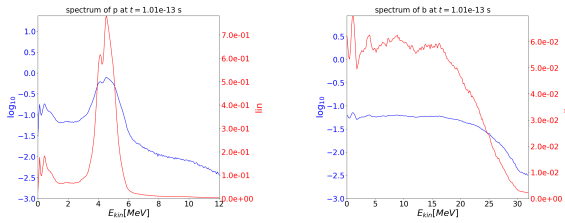


Figure 4: Energy spectra for protons and boron ions generated by a rod with  $R = 25$  nm, which is the small radius regime. The upper plot shows the protons and the lower plot the boron ions. The energy of the protons is sharply peaked. By changing the size and morphology of the nano-structures the ion spectra can be tailored, specifically the boron ion spectra can become much sharper. The simulation parameters are the same as in Fig. 2.

tended to illustrate the flexibility of the concept are depicted in Fig. 5. The figure shows a 2D cylindrical layout and a possible 3D configuration. The accelerator is capable of generating ion flows in the range of  $10^{19} - 10^{20}$  ions with a large range of tunable energies.. The ion energies obtained can be engineered to a large extent. The flows can be generated in much less than a 1 ps. The energy contained in the accelerated ions can range between  $10^{23} - 10^{24}$  eV due to the high conversion efficiency that can range up to 80%.

#### 4. Conclusions

Intense ultra-short laser pulses interacting with tailored nano-structures are capable of generating converging ion flows with  $10^{20}$  ions in a large range of tunable energies on sub-ps time scales.

The properties of these ionic flows may potentially be applied to the design of future reactors for energy production with fuels with sub-MeV activation energies and the formation of hot spots for fusion energy production in the context of isentropic compression schemes.

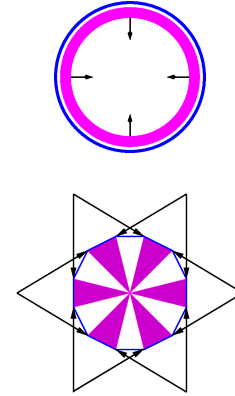


Figure 5: Top view of a hypothetical cylindrical onion shell accelerator - converter layout (top plot). The converter fluid colored in pink is driven by the accelerator colored in blue. The accelerator is capable of generating large ionic currents. A side view on a principal 3D onion shell accelerator - converter layout with its rotational symmetry about the  $x$ -axis is shown in the lower plot. The black arrows illustrate the directions of impinging individual laser pulses.

Specifically, the numerical and experimental investigation of fast reactive flows for fusion energy production in the scope of high activation energy aneutronic fuels like  $p^{11}B$  is our primary goal.

#### 5. Acknowledgements

The present work has been motivated and funded by Marvel Fusion GmbH. We would like to thank the Marvel Fusion team and in particular Christian Bild, Matthias Lienert, Markus Nöth, Gaurav Raj, Michael Touati, and Naveen Yadav.

#### References

- [1] M. Banks, Significant step towards break-even target, *Physics World* 34 (10) (2021) 11ii.
- [2] A. e. a. Zylstra, [Burning plasma achieved in inertial fusion](https://doi.org/10.1038/s41586-021-04281-w), *Nature* 601 (2022) 542–548. doi:10.1038/s41586-021-04281-w. URL <https://doi.org/10.1038/s41586-021-04281-w>
- [3] H. e. a. Abu-Shawareb, [Lawson criterion for ignition exceeded in an inertial fusion experiment](https://doi.org/10.1103/PhysRevLett.129.075001), *Phys. Rev. Lett.* 129 (2022) 075001. doi:10.1103/PhysRevLett.129.075001. URL <https://link.aps.org/doi/10.1103/PhysRevLett.129.075001>
- [4] A. L. e. a. Kritcher, [Design of an inertial fusion experiment exceeding the lawson criterion for ignition](https://doi.org/10.1103/PhysRevE.106.025201), *Phys. Rev. E* 106 (2022) 025201. doi:10.1103/PhysRevE.106.025201. URL <https://link.aps.org/doi/10.1103/PhysRevE.106.025201>
- [5] A. B. e. a. Zylstra, [Experimental achievement and signatures of ignition at the national ignition facility](https://doi.org/10.1103/PhysRevE.106.025202), *Phys. Rev. E* 106 (2022) 025202. doi:10.1103/PhysRevE.106.025202. URL <https://link.aps.org/doi/10.1103/PhysRevE.106.025202>
- [6] U. D. of Energy, [Doe national laboratory makes history by achieving fusion ignition](https://www.llnl.gov/news/national-ignition-facility-achieves-fusion-ignition), retrieved on Dec. 14, 2022 (Dec 2022).
- [7] B. Bishop, [National ignition facility achieves fusion ignition](https://www.llnl.gov/news/national-ignition-facility-achieves-fusion-ignition), retrieved Dec. 14, 2022 (Dec 2022). URL <https://www.llnl.gov/news/national-ignition-facility-achieves-fusion-ignition>

- [8] K. Chang, [Scientists achieve nuclear fusion breakthrough with blast of 192 lasers](#), retrieved Dec. 14, 2022 (Dec 2022).  
URL <https://www.nytimes.com/2022/12/13/science/nuclear-fusion-energy-breakthrough.html>
- [9] D. Clercy, [With historic explosion, a long sought fusion breakthrough](#), retrieved Dec. 14, 2022 (Dec 2022).  
URL <https://www.science.org/content/article/historic-explosion-long-sought-fusion-breakthrough>
- [10] S. Atzeni, J. Meyer-ter Vehn, *The physics of inertial fusion: beam plasma interaction, hydrodynamics, hot dense matter*, Vol. 125, OUP Oxford and citations therein, 2004.
- [11] L. Fedeli, A. Formenti, L. Cialfi, A. Pazzaglia, M. Passoni, *Ultra-intense laser interaction with nanostructured near-critical plasmas*, *Scientific reports* 8 (1) (2018) 1–10.
- [12] Z. Léczy, A. Andreev, [Laser-induced extreme magnetic field in nanorod targets](#), *New Journal of Physics* 20 (3) (2018) 033010. doi:10.1088/1367-2630/aaaff2.  
URL <https://dx.doi.org/10.1088/1367-2630/aaaff2>
- [13] J. F. Ong, P. Ghenuche, K. A. Tanaka, [Electron transport in a nanowire irradiated by an intense laser pulse](#), *Phys. Rev. Research* 3 (2021) 033262. doi:10.1103/PhysRevResearch.3.033262.  
URL <https://link.aps.org/doi/10.1103/PhysRevResearch.3.033262>
- [14] L. Fedeli, A. Formenti, L. e. a. Cialfi, [Ultra-intense laser interaction with nanostructured near-critical plasmas](#), *Sci. Rep.* 8 (2021) 3834. doi:10.1038/s41598-018-22147-6.  
URL <https://doi.org/10.1038/s41598-018-22147-6>
- [15] A. Curtis, R. Hollinger, C. Calvi, S. Wang, S. Huanyu, Y. Wang, A. Pukhov, V. Kaymak, C. Baumann, J. Tinsley, V. N. Shlyaptsev, J. J. Rocca, [Ion acceleration and d-d fusion neutron generation in relativistically transparent deuterated nanowire arrays](#), *Phys. Rev. Research* 3 (2021) 043181. doi:10.1103/PhysRevResearch.3.043181.  
URL <https://link.aps.org/doi/10.1103/PhysRevResearch.3.043181>
- [16] J. Park, R. Tommasini, R. Shepherd, R. A. London, C. Bargsten, R. Hollinger, M. G. Capeluto, V. N. Shlyaptsev, M. P. Hill, V. Kaymak, C. Baumann, A. Pukhov, D. Cloyne, R. Costa, J. Hunter, S. Maricle, J. Moody, J. J. Rocca, [Absolute laser energy absorption measurement of relativistic 0.7 ps laser pulses in nanowire arrays](#), *Physics of Plasmas* 28 (2) (2021) 023302. arXiv:<https://doi.org/10.1063/5.0035174>, doi:10.1063/5.0035174.  
URL <https://doi.org/10.1063/5.0035174>
- [17] D. Strickland, G. Mourou, *Compression of amplified chirped optical pulses*, *Optics communications* 55 (6) (1985) 447–449.
- [18] C. N. Danson, C. Haefner, J. Bromage, T. Butcher, J.-C. F. Chanteloup, E. A. Chowdhury, A. Galvanauskas, L. A. Gizzi, J. Hein, D. I. Hillier, et al., *Petawatt and exawatt class lasers worldwide*, *High Power Laser Science and Engineering* 7 (2019).
- [19] H. Ruhl, G. Korn, [A laser-driven mixed fuel nuclear fusion reactor concept](#) (Feb. 2022). doi:10.48550/arXiv.2202.03170.
- [20] R. Craxton, K. Anderson, T. Boehly, V. Goncharov, D. Harding, J. Knauer, R. McCrory, P. McKenty, D. Meyerhofer, J. Myatt, et al., *Direct-drive inertial confinement fusion: A review*, *Physics of Plasmas* 22 (11) (2015) 110501.